

Heterogeneous & Homogeneous & Bio- & Nano-

CHEM**CAT**CHEM

CATALYSIS

Accepted Article

Title: Facile fabrication of ultrasmall copper species confined in mesoporous silica for chemo-selective and stable hydrogenation ethylene carbonate derived from CO₂

Authors: Ligu Wang

This manuscript has been accepted after peer review and appears as an Accepted Article online prior to editing, proofing, and formal publication of the final Version of Record (VoR). This work is currently citable by using the Digital Object Identifier (DOI) given below. The VoR will be published online in Early View as soon as possible and may be different to this Accepted Article as a result of editing. Readers should obtain the VoR from the journal website shown below when it is published to ensure accuracy of information. The authors are responsible for the content of this Accepted Article.

To be cited as: *ChemCatChem* 10.1002/cctc.201800828

Link to VoR: <http://dx.doi.org/10.1002/cctc.201800828>

Facile fabrication of ultrasmall copper species confined in mesoporous silica for chemo-selective and stable hydrogenation ethylene carbonate derived from CO₂

Chanjuan Zhang,^[a,b,c,d] Ligu Wang^{*[a,c,d]}, Jiaju Liu,^[a] Yanmi Yang,^[a] Peng He,^[a] Yan Cao,^[a] Jiaqiang Chen,^[a] Huiquan Li^{*[a,c,d]}

Abstract: The hydrogenation of ethylene carbonate to co-produce commodity methanol and ethylene glycol has attracted growing interests due to the potential chemical utilization of CO₂ in large scale. In this work, we report a novel and facile protocol for the preparation the mesoporous Cu@SiO₂ catalysts and successfully applied the as-synthesized catalysts in the hydrogenation of ethylene carbonate. The catalysts were characterized by means of N₂ physisorption, N₂O titration, XRD, FT-IR, H₂-TPR, TEM and XPS (XAES) in details. In particular, this strategy was demonstrated an effective method in fabricating the unique flower-like mesoporous Cu@SiO₂ with sub-2.0 nm ultrasmall Cu particles. The results revealed that the involvement of β -cyclodextrin improved the Cu dispersion and facilitated exposing more copper active sites, which also indicated that the confined catalyst inhibiting the sintering of copper particles. Meanwhile, the stability of the attained catalyst was superior with the modification of carbon. Importantly, among the catalysts tested in the hydrogenation of ethylene carbonate, 25Cu@SiO₂- β -P with appropriate copper loading as well as moderate Cu⁺ ratio exhibited superior catalytic performance. Accordingly, the synergistic effect between the Cu⁺ and metallic Cu⁰ species was considered to be the crucial for obtaining better catalytic activity.

Introduction

Huge emission of carbon dioxide into the atmosphere by human activity has imposed significant influence on global warming. In

recent years, the chemical utilization of carbon dioxide as an important feedstock for the syntheses of fuels, materials and chemicals has drawn great attentions.^[1-2] In this regard, the strategy for converting CO₂ into value-added oxygenates are being paid intensive study.^[3-6] Recently, the catalytic hydrogenation of CO₂ derivations, e.g. carbonates, carbamates and urea, provides an alternative approach for the efficient transformation of CO₂ indirectly.^[7-9] Particularly, methanol is the important raw material for the production of oxygen-containing chemicals and fuels, e.g. formaldehyde, acetic acid, olefins, which is also expected the excellent hydrogen carrier.^[10-14] Nevertheless, the direct utilization of CO₂ to methanol requires harsh reaction conditions due to its kinetic inertness and the high activation energy for cleavage of C=O bonds in CO₂ molecular. Meanwhile, the direct process usually suffers from low product yield owing to the thermodynamic limitations. In order to enhance the utilization efficiency, indirect route has provided alternative pathway and demonstrated promising application.

In recent years, the hydrogenation reaction of ethylene carbonate (EC) to co-produce important commodities of methanol and ethylene glycol (EG) has attracted special concerns due to the merits of environmentally friendliness, atomic economy and low energy consumption.^[15-17] Therefore, many researchers have devoted great efforts for developing effective catalysts. The homogeneous princer-type Ru^{II} complex catalyst with high efficiency was applied for the hydrogenation of EC.^[18-19] On account of the convenient catalyst recovery, much work was devoted to develop effective and easily recyclable heterogeneous catalysts for the chemoselective hydrogenation of EC. Because the unique property demonstrated in the selective hydrogenation of carbonyl bonds, copper-based catalysts were studied extensively in the catalytic hydrogenation of ester for the synthesis of alcohols, thus ensuring the good selectivity of target products.^[20-24] As reported in previous literatures for the analogous reaction, Cu/SiO₂ catalysts as a versatile hydrogenation catalyst showed an excellent application in the hydrogenation of dimethyl oxalate to EG or ethanol.^[25-26] In particular, heterogeneous copper-based catalysts, e.g., CuCr₂O₄,^[27] Cu-SiO₂-PG,^[28] Cu/HMS,^[29] Cu/SBA-15^[20] and Cu/SiO₂-AE^[16] were investigated for EC hydrogenation to co-produce methanol and EG, and displayed relatively good catalytic performance. Among these catalysts tested, a maximum turnover frequency (TOF) of 776 mg_{EC}·g_{cat}⁻¹·h⁻¹ was obtained over Cu/SBA-15. However, more effective, low-cost heterogeneous catalysts with high efficiency are highly desired. As also proposed,^[25-28] the size of the copper particles are considered to be the crucial factors in hydrogenation reaction. Therefore, the protocol for the preparation of the copper-based catalysts with finely tuned particles is of great significance.^[20,26] Recently, Yao et al reported

[a] C. Zhang, Dr. L. Wang, J. Liu, Y. Yang, Dr. P. He, Dr. Y. Cao, J. Chen, Prof. Dr. H. Li, CAS Key Laboratory of Green Process and Engineering, Institute of Process Engineering, Chinese Academy of Sciences, 1 North 2nd Street, Zhongguancun, Haidian District, Beijing, PR China

[b] C. Zhang, Chemical and Biochemical Engineering, Technical University of Denmark, Building 229, 2800 Kgs. Lyngby, Denmark

[c] C. Zhang, Dr. L. Wang, Prof. Dr. H. Li, Sino-Danish College, University of Chinese Academy of Sciences, No.19(A) Yuquan Road, Shijingshan District, Beijing, P.R.China

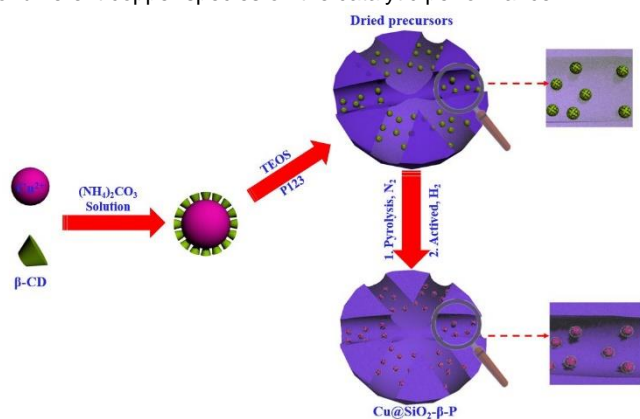
[d] C. Zhang, Dr. L. Wang, Prof. Dr. H. Li, Sino-Danish center for Education and Research, University of Chinese Academy of Sciences, No.19(A) Yuquan Road, Shijingshan District, Beijing, P.R.China

Supporting information for this article is given via a link at the end of the document. **(Please delete this text if not appropriate)**

FULL PAPER

a robust copper-based catalysts with the introduction of low-cost dextrin and employed it in the system of dimethyl oxalate hydrogenation successfully.^[30] The catalytic activity and stability of the as-prepared catalysts were enhanced greatly with the formation of dextrin-coating. Meanwhile, the deactivation reason responsible for the stability was also highly concerned for giving insights into stabilizing mechanism.^[16, 20, 28]

In this work, we provide a facile method shown in Scheme 1 of one-step hydrolysis precipitation with the aid of β -cyclodextrin and templating agent of P123 to prepare uniformly dispersed copper-based catalysts for the first time and apply the as-prepared catalysts in hydrogenation of ethylene carbonate derived from CO_2 . Furthermore, the structures and the physicochemical properties of catalysts were systematically characterized by different techniques, e.g., N_2 physisorption, ICP-AES, N_2O titration, FT-IR, XRD, H_2 -TPR, TEM, XPS and XAES. Moreover, the catalytic performance, the effects of reaction parameters and the reusability of catalyst were also investigated. In addition, the correlation between the catalytic performance and the unique roles of Cu^0 and Cu^+ sites was also studied to elucidate the effect of different copper species on the catalytic performance.



Scheme 1. Schematic illustration for the fabrication of carbon promoted catalyst $\text{xCu@SiO}_2\text{-}\beta\text{-P}$

Results and Discussion

Catalyst characterization

N_2 physisorption, ICP-AES and N_2O titration

N_2 physisorption isotherms and the pore size distribution curves of $\text{xCu@SiO}_2\text{-}\beta\text{-P}$ and $25\text{Cu@SiO}_2\text{-P}$ catalysts were depicted in Fig. 1, and the physico-chemical properties of these samples were summarized in Table 1. According to the N_2 physisorption isotherms with the IUPAC classification, type IV with H1-type hysteresis loops was observed for all these samples, suggesting the mesoporous structures were successfully fabricated.^[31] For $\text{xCu@SiO}_2\text{-}\beta\text{-P}$ catalysts, the surface area of $\text{xCu@SiO}_2\text{-}\beta\text{-P}$ catalysts increased firstly when Cu loadings lower than 25%, while it declined when Cu loadings further elevated to 35%. Moreover, the pore shape of the $\text{xCu@SiO}_2\text{-}\beta\text{-P}$ catalysts changed from “spherical” to “slit-like” with increasing the copper loading.^[16] As shown in Fig. 1b, the pore sizes of $\text{xCu@SiO}_2\text{-}\beta\text{-P}$

($\text{x}\leq 25\%$) and $25\text{Cu@SiO}_2\text{-P}$ catalysts distributed between 10-30 nm and the peak of pore distribution shifted right with copper loadings ($\text{x}<25\%$), while the amounts of micropores in $\text{xCu@SiO}_2\text{-}\beta\text{-P}$ ($\text{x}\geq 25\%$) showed a dramatic decrease after the nominal copper-loading over 25%, which was also observed in the literature.^[32] The declined pore sizes of $\text{xCu@SiO}_2\text{-}\beta\text{-P}$ catalysts ($\text{x}>35\%$) implied that the micropores were blocked by the larger copper nanoparticles or the formation process of micropores was influenced by the excess copper loading, which was consistent with the N_2 physisorption isothermal curves of catalysts. The relatively larger surface area of $105.6\text{ m}^2/\text{g}$ was obtained for $25\text{Cu@SiO}_2\text{-}\beta\text{-P}$ with appropriate copper loading. As expected, the enlarged surface area for $25\text{Cu@SiO}_2\text{-P}$ revealed that P123 as templating agent facilitates obtaining a larger surface area. In addition, the distribution of average pore sizes with the copper loading showed unregular tendency. Furthermore, compared with the $\text{xCu@SiO}_2\text{-}\beta\text{-P}$ catalysts with different copper loadings and $25\text{Cu@SiO}_2\text{-P}$ catalyst, the larger pore size of $0.43\text{ cm}^3/\text{g}$ was obtained over $25\text{Cu@SiO}_2\text{-}\beta\text{-P}$ due to the combination of β -cyclodextrin and P123. ICP-AES results demonstrated that the actual copper contents of catalysts were close to the nominal value, indicating the copper is almost completely deposited on the catalyst. There was another interesting phenomenon that the actual copper contents increased sharply while the nominal value over 25%, the copper content difference between actual and nominal contents indicates that the excess copper inhibits the formation of the spherical structure. Copper dispersion of $\text{xCu@SiO}_2\text{-}\beta\text{-P}$ and $25\text{Cu@SiO}_2\text{-P}$ catalysts were also determined by N_2O titration, which were summarized in Table 1. Obviously, the Cu dispersion of $15\text{Cu@SiO}_2\text{-}\beta\text{-P}$ is 26.8% which decreased with the increment of copper loading, and it can be speculated that the excess copper content influences the formation of catalyst which is consistent with the assumption from ICP-CAS results. On the contrast, compared to that of $25\text{Cu@SiO}_2\text{-}\beta\text{-P}$ catalyst (16.1%), the copper dispersion of $25\text{Cu@SiO}_2\text{-P}$ without the introduction of β -cyclodextrin decreased to 10.0%. The atomic ratios of Cu/Si on the surface of catalysts were also measured by XPS and summarized in Tab. 1. The copper ratio initially increased with the copper loading of $\text{xCu@SiO}_2\text{-}\beta\text{-P}$ catalysts ($\text{x}\leq 25\%$) and subsequently decreased to 0.033 of $35\text{Cu@SiO}_2\text{-}\beta\text{-P}$ from the highest value 0.047 of $25\text{Cu@SiO}_2\text{-}\beta\text{-P}$. Furthermore, the introduction of β -cyclodextrin promoted the copper ratio on the surface of catalysts. The tendency of the atomic ratios Cu/Si matched well with that of BET surface area. Combining with the actual copper loading from ICP-AES and the copper dispersity from N_2O titration, copper dispersity decreased with copper loadings, while the atomic ratio of Cu/Si on the surface of catalysts increased with copper loading ($\text{x}\leq 25\%$), indicating the catalysts with moderate copper contents were beneficial for exposing more copper active sites. Meanwhile, the relative lower copper contents led to a higher dispersity. Moreover, both the results of copper dispersity and the atomic ratio of Cu/Si for $25\text{Cu@SiO}_2\text{-}\beta\text{-P}$ and $25\text{Cu@SiO}_2\text{-P}$ catalysts suggested that β -cyclodextrin played a significant role in promoting the copper dispersity.

FULL PAPER

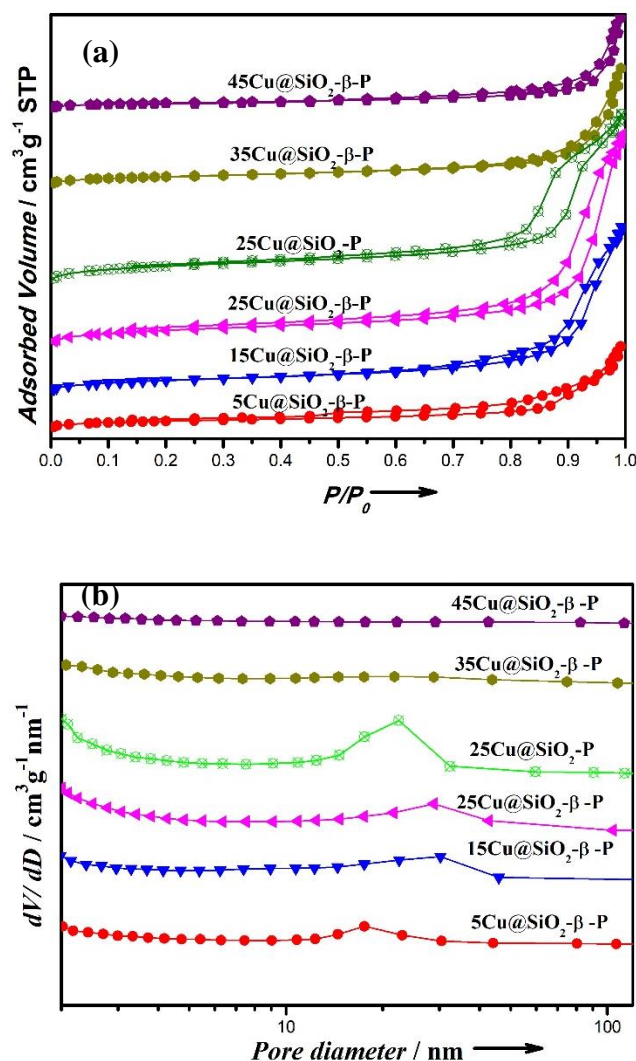


Figure 1. (a) N_2 physisorption isotherms (b) pore size distributions of $x\text{Cu}@SiO_2-\beta\text{-P}$ catalysts, $x=5, 15, 25, 35$ and 45 and $25\text{Cu}@SiO_2\text{-P}$.

Table 1. Physico-chemical properties of $x\text{Cu}@SiO_2-\beta\text{-P}$ and $25\text{Cu}@SiO_2\text{-P}$ catalysts.

Catalyst	Cu loading ^[a] (%)	$S_{\text{BET}}^{\text{[b]}}$ (m^2g^{-1})	$D_{\text{Cu}}^{\text{[c]}}$ (%)	$d_{\text{pore}}^{\text{[b]}}$ (nm)	$V_{\text{pore}}^{\text{[b]}}$ (cm^3g^{-1})	$\text{Cu}/\text{Si}^{\text{[d]}}$ (mol ratio)
$5\text{Cu}@SiO_2-\beta\text{-P}$	4.7	54.7	48.0	17.5	0.17	0.025
$15\text{Cu}@SiO_2-\beta\text{-P}$	14.9	79.2	26.8	30.2	0.34	0.045
$25\text{Cu}@SiO_2-\beta\text{-P}$	25.9	105.6	16.1	28.8	0.43	0.047
$35\text{Cu}@SiO_2-\beta\text{-P}$	40.9	57.6	14.8	43.8	0.24	0.033
$45\text{Cu}@SiO_2-\beta\text{-P}$	58.8	31.7	-	23.1	0.18	-
$25\text{Cu}@SiO_2\text{-P}$	25.5	128.6	10.0	22.4	0.36	0.032

[a] Measured by ICP-AES. [b] Obtained by N_2 physisorption. [c] Determined by N_2O titration. [d] Attained by XPS

TGA

TGA analysis of beta-cyclodextrin was carried out to confirm the existence of residual carbon from beta-cyclodextrin, which was shown in Fig. S1. Obviously, there was two main weight losses from ambient temperature to 400°C in pure nitrogen atmosphere. The first loss of 13.4 % could be ascribed to the removal of absorbed water when the temperature was lower than 120°C . Another drastic weight loss started at around 300°C and ended at around 400°C with obvious heat adsorption of 320°C , and the majority weight loss of 74.8% indicated the thermal decomposition of beta-cyclodextrin which was consistent with the previous report,^[33] indicating beta-cyclodextrin was primarily eliminated before 450°C . Therefore, we deduced that the residual carbon formed in the as-prepared catalysts after the thermal decomposition in pure nitrogen atmosphere at 450°C . Accordingly, it can be speculated that beta-cyclodextrin was eliminated primarily after the calcination process at 450°C for 4h and the residual carbon was introduced in the as-prepared catalysts successfully. This phenomenon was also observed in the reference.^[30]

FT-IR

The FT-IR spectra of the dried precursors and the reduced catalysts of $x\text{Cu}@SiO_2-\beta\text{-P}$ and $25\text{Cu}@SiO_2\text{-P}$ were illustrated in Fig.2. For the dried precursors, two obvious peaks of 1080 cm^{-1} and 1250 cm^{-1} were observed in the all dried precursors of $x\text{Cu}@SiO_2-\beta\text{-P}$, which can be attributed to the vibration modes of Si-O bands. Besides, both the symmetric stretching vibration peak of 800 cm^{-1} and the bending vibration bands of 457 cm^{-1} reflected the existence of Si-O-Si bands. The bands at 620 cm^{-1} and 580 cm^{-1} ascribed to the stretching vibration of Cu-O bond in monoclinic CuO. The obvious presence of 1385 cm^{-1} and 1502 cm^{-1} when the copper loading above 15% can be assigned to the NO_3 and CO_3 groups from $\text{Cu}_2(\text{OH})_3\text{NO}_3$ and $\text{Cu}_2(\text{OH})_2\text{CO}_3$,^[34] respectively, implying the formation of copper complexes. The presence of 1502 cm^{-1} peak in dried precursor was observed, suggesting that the existence of mode ν_3 of interlayer carbonate species.^[35] The peak around 1027 cm^{-1} can be assigned to the formation of copper phyllosilicate, which was considered to be originated from the strong interaction between copper species and silica support.^[16,36] It can be concluded that the dried precursors $x\text{Cu}@SiO_2-\beta\text{-P}$ contained $\text{Cu}_2(\text{OH})_3\text{NO}_3$, $\text{Cu}_2(\text{OH})_2\text{CO}_3$ and copper phyllosilicate, while that of $25\text{Cu}@SiO_2\text{-P}$ catalyst contained copper phyllosilicate as well as $\text{Cu}_2(\text{OH})_3\text{NO}_3$. The peaks of 1502 cm^{-1} and 1385 cm^{-1} disappeared for the reduced catalysts, as shown in Fig. 2b, indicating that the NO_3 and CO_3 groups were destroyed in the subsequent calcination and reduction processes, while there still was an obvious peak on the curve of $45\text{Cu}@SiO_2-\beta\text{-P}$ which implied that the excess copper loading disturbed the completed reduction process. The diverse copper species in the precursor may impose a great effect on the variation of copper species in the reduced catalyst.

FULL PAPER

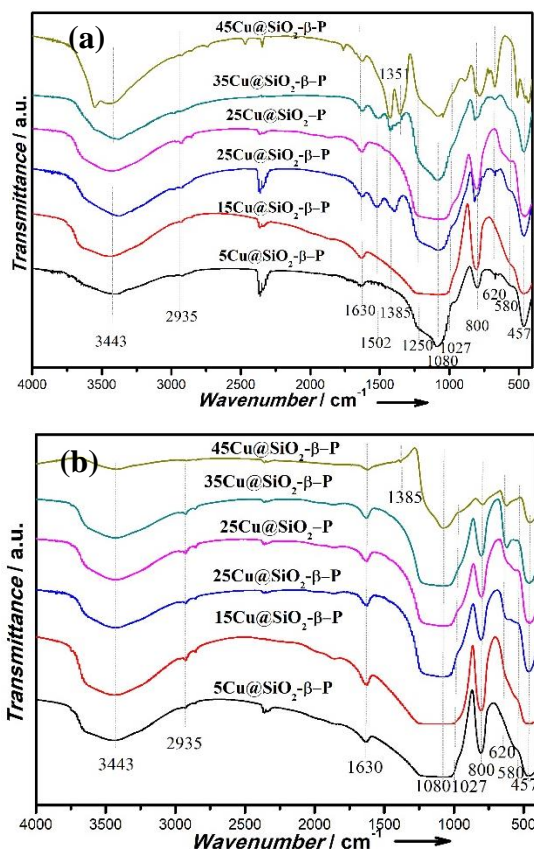


Figure 2. FT-IR of (a) the dried precursors, (b) reduced catalysts of $x\text{Cu}@SiO_2\text{-}\beta\text{-P}$ and $25\text{Cu}@SiO_2\text{-P}$.

XRD

Fig. 3 showed the XRD patterns of the dried precursors and the reduced catalysts of $x\text{Cu}@SiO_2\text{-}\beta\text{-P}$ and $25\text{Cu}@SiO_2\text{-P}$. As shown in Fig. 3a, only one characteristic diffraction peak at 2θ of 22.8° assignable to amorphous SiO_2 was observed for $5\text{Cu}@SiO_2\text{-}\beta\text{-P}$. For the catalysts with copper loadings in the region of 15% and 35%, there are distinguished diffraction peaks at 2θ of 14.7° , 17.6° , 24.2° , 17.6° , 31.3° and 36.6° assigned to cupric subcarbonate $Cu_2(OH)_2CO_3$ could be observed. It can be clearly found that the corresponding peak intensities increased with the copper loadings, indicating the enhanced crystallinity. Furthermore, the new crystal phase appeared when copper loading greater than 25%, and the diffraction peaks at 2θ of 13.0° – 63.0° ascribable to the monoclinic $Cu_2(OH)_3NO_3$.^[37] For the reduced catalyst of $x\text{Cu}@SiO_2\text{-}\beta\text{-P}$ and $25\text{Cu}@SiO_2\text{-P}$, as presented in Fig. 3b, the weak diffraction peaks of $Cu_2(OH)_3NO_3$ and $Cu_2(OH)_2CO_3$ existed in the dried precursors disappeared completely after reduction. Specifically, for the $x\text{Cu}@SiO_2\text{-}\beta\text{-P}$ samples with x above 5%, the presence of diffraction peaks at 2θ of 36.5° , 43.4° and 61.6° could be indexed to the (111), (200) and (220) crystal planes of Cu_2O , respectively. Meanwhile, the evident diffraction peaks at 2θ of 50.6° and 74.0° could be assigned to the (220) and (220) crystal planes of metallic fcc Cu, respectively. The diffraction peaks for Cu_2O and Cu^0 become more intensive when

increasing the copper loading, indicating relatively larger particle size were formed with the increment of copper content. Besides, there was no detectable diffraction peak of CuO , suggesting that all of the Cu^{2+} was primarily reduced to copper species with low valences, i.e. Cu^0 or Cu^+ after reduction.^[27,38-39] Moreover, the increased intensity of diffraction peaks with increasing copper loading suggested the size of copper particles also increased with copper loadings. The evolution of the copper species during the preparation process is in agreement with the results of FT-IR. These results proved the Cu_2O and metallic Cu species were well dispersed on silica support, especially for the samples with lower copper loadings, which is in agreement of N_2O titration result.

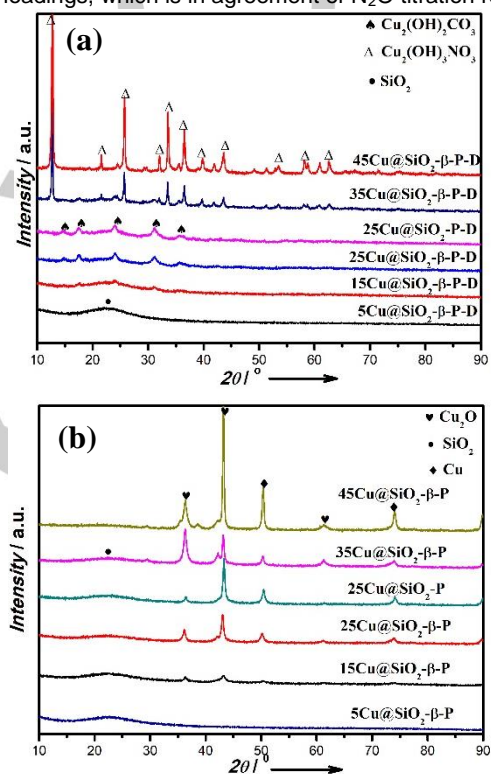


Figure 3. XRD of (a) dried precursors, (b) reduced catalysts of $x\text{Cu}@SiO_2\text{-}\beta\text{-P}$.

H₂-TPR

Fig. 4 showed the H_2 -TPR profile of the $x\text{Cu}@SiO_2\text{-}\beta\text{-P}$ and $25\text{Cu}@SiO_2\text{-P}$ catalysts. All of the catalysts exhibited a symmetrical reduction peak. The onset of the reduction peaks of these catalysts centered at about 529 K–546 K could be primarily ascribable to the collective reduction of copper phyllosilicate and well dispersed CuO particles.^[20,40] The TPR reduction peak gradually shifted to higher temperature regions with the augment of Cu content, presumably ascribed to the larger CuO_x particle size with deteriorated dispersion or strongly interactions between copper species and silica support at higher copper loading. Moreover, compared to $25\text{Cu}@SiO_2\text{-}\beta\text{-P}$, the reduction peak of $25\text{Cu}@SiO_2\text{-}\beta\text{-P}$ with the same copper loading shifted towards the lower temperature regions, suggesting that the introduction of

FULL PAPER

β -cyclodextrin is beneficial for enhancing the reducibility of oxidized copper species. It is generally accepted that the entire reduction of Cu^+ species to metallic Cu^0 at the premise of high reduction temperature above 873 K.^[16] In this case, after reduction, copper phyllosilicate or Cu-O-Si was also transformed into Cu^+ , while CuO was reduced to metallic Cu^0 species,^[16,20,39] which is consistent with the findings from FT-IR and XRD.

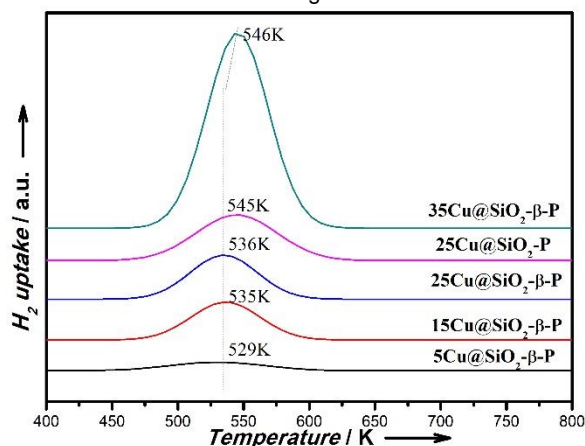


Figure 4. H_2 -TPR of the catalysts of $x\text{Cu}@/\text{SiO}_2\text{-}\beta\text{-P}$, $x=5, 15, 25, 35$ and $25\text{Cu}@/\text{SiO}_2\text{-P}$.

TEM

The catalyst morphology and particle size distributions of $x\text{Cu}@/\text{SiO}_2\text{-}\beta\text{-P}$ and $25\text{Cu}@/\text{SiO}_2\text{-P}$ were shown in Fig. 5 and Fig S2. The morphology was controlled to be nanoflower-like structure. The distinct mesoporous channel structure can be observed in Fig 5a-b and Fig S2, which is exclusively favorable for improving copper dispersion and promoting the catalytic performance in EC hydrogenation. The histograms of particle size distributions for the different copper loading were also obtained by measuring particles from TEM images. As a result, the average particle diameters of $x\text{Cu}@/\text{SiO}_2\text{-}\beta\text{-P}$ catalysts increased with the copper loading, and the average particle diameters were 0.9 nm, 1.0 nm, 1.6 nm, 1.8 nm and 9.6 nm with $x=5, 15, 25, 35$ and 45, respectively. The particle size increased from 1.8 nm to 9.6 nm rapidly, implying the excess copper loading impacted the generation of the particles and lead to the aggregation of particles. In combination with the results from XRD shown in Fig. 3b, there was no detectable peak of metallic Cu and Cu_2O in $5\text{Cu}@/\text{SiO}_2\text{-}\beta\text{-P}$ with 5% copper content, possibly because that all of the copper particles sizes were lower than 2 nm. Actually, as also reported by Tomishige et al.,^[37] the peaks of copper crystallites were difficult to be detected by XRD when the copper particles were lower than 2 nm. Whereas, the peaks related to Cu^0 and Cu_2O appeared when copper loading was 15% and the peak intensities further enhanced with the increase of copper loadings. As shown in Fig. 3b and Fig. 5, the copper particle sizes increased with copper loadings and there was a dramatic increase when copper loadings over 35%. The appearance of peaks ascribed to Cu_2O were observed in 15-35 $\text{Cu}@/\text{SiO}_2\text{-}\beta\text{-P}$ catalysts, indicating that the larger copper particle sizes ($d \geq 2\text{nm}$) presented in 15-

35 $\text{Cu}@/\text{SiO}_2\text{-}\beta\text{-P}$ catalyst. Although the mean particle sizes lower than 2 nm, the large particles with diameter larger than 2 nm were also observed and collected in the distribution of copper particles by TEM. Meanwhile, the existence of minority particles with larger sizes could not be completely excluded, which possibly also contributed to the peaks of copper species in XRD spectra. For 45 $\text{Cu}@/\text{SiO}_2\text{-}\beta\text{-P}$, the mean copper particle size was 9.6 nm, which can be obviously detected by XRD. Therefore, it can be speculated that the copper particle sizes of $x\text{Cu}@/\text{SiO}_2\text{-}\beta\text{-P}$ increased with copper-loadings. Moreover, the peak intensities of Cu and Cu_2O increased with the copper loadings, implying the increase of copper particles sizes in $x\text{Cu}@/\text{SiO}_2\text{-}\beta\text{-P}$ catalysts, which was consistent with the results obtained from TEM. Notably, the statistical results revealed that average particle sizes mainly distributed in the regions of sub-2 nm if the copper loading less than 35%, indicating the preparation method used in this study has provided an effective protocol for controllable syntheses of the catalysts with ultras-small Cu nanoparticles in uniform distribution. In combination of the results demonstrated in N_2 physisorption, N_2O titration and H_2 TPR, the introduction of β -cyclodextrin is favorable for the copper dispersion and improved the uniformity of particle size distribution.

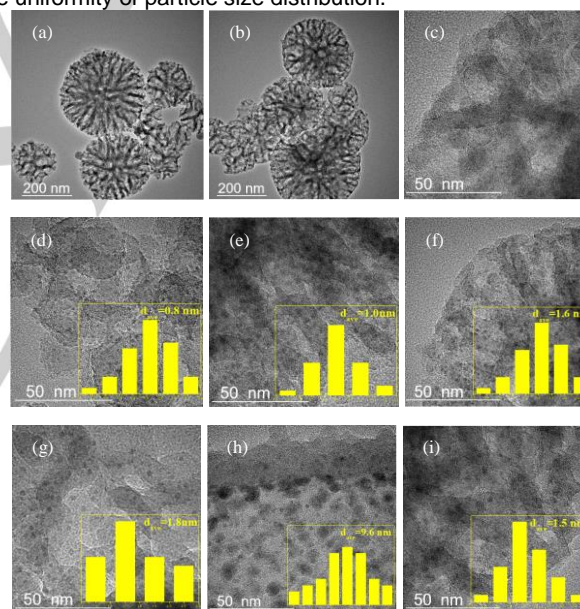


Figure 5. TEM images for the catalyst morphology: (a) $15\text{Cu}@/\text{SiO}_2\text{-}\beta\text{-P}$, (b) $25\text{Cu}@/\text{SiO}_2\text{-}\beta\text{-P}$, the particle size distribution of (c) the dry precursor of $25\text{Cu}@/\text{SiO}_2\text{-}\beta\text{-P}$, the reduced $x\text{Cu}@/\text{SiO}_2\text{-}\beta\text{-P}$ catalysts: (d) $x=5$, (e) $x=15$, (f) $x=25$, (g) $x=35$ (h) $x=45$, (i) $25\text{Cu}@/\text{SiO}_2\text{-P}$.

Element mapping by energy-dispersive X-ray (EDX)

EDX spectroscopy showed that elemental copper and carbon were uniformly distributed on mesoporous silica, as presented in Fig 6. Furthermore, the co-existence copper and carbon illustrated these two species were synchronously distributed, in which the residual carbon was deemed to be originated from β -cyclodextrin during the carbonization process in inert atmosphere.

FULL PAPER

In combination of TEM images with the result from EDX mapping, it can be concluded that the one-step method by hydrolysis precipitation is an excellent protocol for preparing the catalyst with high-dispersed Cu species and petal morphology, which was considered to facilitate inhibiting the agglomeration of copper species and stabilize the copper species in some extent. From the results aforementioned, it can be deduced that the Cu species are also decorated by residual carbon and confined in mesoporous silica channels.

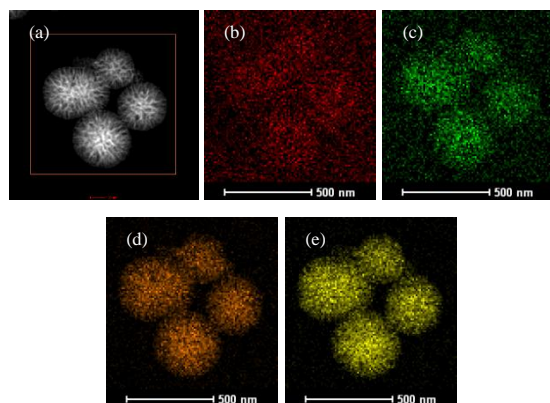


Figure 6. EDX mapping of the reduced catalyst 25Cu@SiO₂-β-P: (a) Overall state, (b) C-mapping, (c) Cu-mapping, (d) O-mapping, (e) Si-mapping.

XPS

The surface properties of chemical states and compositions of the reduced xCu@SiO₂-β-P and 25Cu@SiO₂-P catalysts were achieved by XPS and XAES illustrated in Fig.7, and the relevant quantitative data were collected in Table 2. The slim binding energy range of Cu 2p_{3/2} without obvious satellite peaks of Cu²⁺ was determined from 933.1 eV to 933.9 eV except the binding energy of 45Cu@SiO₂-β-P which indicated the uncompleted reduction of higher copper loading catalyst and was consistent with the result of FT-IR and TEM. The variation of the Cu 2p_{3/2} binding energy values of xCu@SiO₂-β-P suggested the different interactions between the copper species and the supports. Owing to the limitation of XPS measurement, XAES was performed to distinguish Cu⁰ and Cu⁺ species. The asymmetric and broad peaks of xCu@SiO₂-β-P catalysts were deconvoluted into two overlapping Cu LMM Auger kinetic energy peaks at ca. 912 eV and 915 eV, which represented Cu⁺ and Cu⁰, respectively.^[41-42] According to the previous reports,^[16,39] Cu⁺ could be ascribed to the reduction of copper phyllosilicate, and Cu⁰ was derived from the reduction of CuO. As summarized in Table 2, the proportion of Cu⁺/(Cu⁰+Cu⁺) increased with the copper loading less than 25%, while the proportion of Cu⁺ decreased from 0.54 to 0.43 at copper loading of 35%. Among the catalysts tested, the maximum Cu⁺ proportion of 0.54 was attained over 25Cu@SiO₂-β-P with the medium copper loading of 25%. Compared to 25Cu@SiO₂-P, 25Cu@SiO₂-β-P with the introduction β-cyclodextrin greatly influenced the ratio of Cu⁺ to the total amount of (Cu⁰+Cu⁺),

resulting in a balanced copper species distribution. The results from XPS and XAES demonstrated that Cu⁰ and Cu⁺ co-existed on the surfaces of these copper-based catalysts with varied proportions.

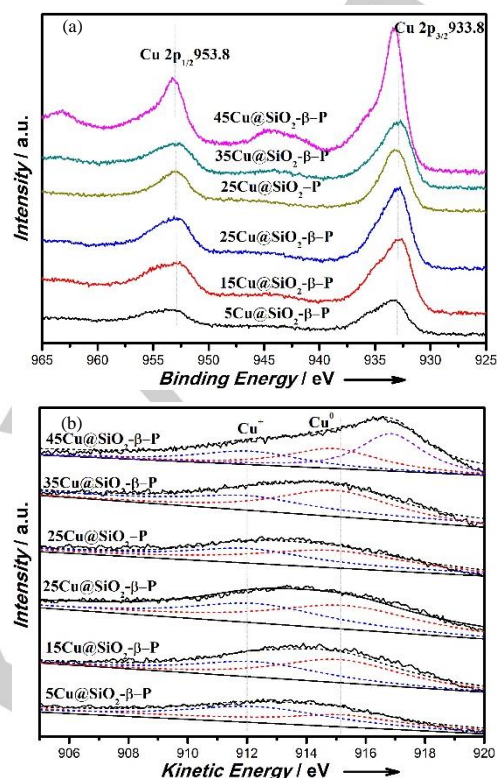


Figure 7. (a) Cu 2p XPS and (b) Cu LMM XAES spectra of the reduced xCu@SiO₂-β-P catalysts.

Table 2. Assignments of copper species in copper-based catalysts attained from Cu LMM XAES spectra.

Catalyst	Binding Energy (eV)		Kinetic Energy (eV)		Cu ⁺ /(Cu ⁰ +Cu ⁺) (mol ratio)
	Cu 2p _{3/2}	Si 2p	Cu ⁺	Cu ⁰	
5Cu@SiO ₂ -β-P	933.7	103.3	912.2	914.8	0.29
15Cu@SiO ₂ -β-P	932.6	103.1	911.8	914.8	0.29
25Cu@SiO ₂ -β-P	933.7	103.3	912.1	915.3	0.54
35Cu@SiO ₂ -β-P	933.1	103.1	912.0	915.0	0.43
45Cu@SiO ₂ -β-P	933.1	103.2	912.1	914.9	0.44
25Cu@SiO ₂ -P	933.9	103.2	912.1	915.1	0.36

Catalyst performance

The catalytic performance tests of xCu@SiO₂-β-P and 25Cu@SiO₂-P catalysts for the hydrogenation of ethylene carbonate was carried out under 453 K for 4 h, and the results were summarized in Table 3. Merely 9.4% EC conversion with 95.2% EG and 11.0% methanol selectivities was obtained over 5Cu@SiO₂-β-P, entry 1. The catalytic activity increased gradually with further increasing the copper loadings to maximum 45% at

FULL PAPER

the identical interval of 10%, entries 2-5. Among them, the relatively moderate catalytic activity, i.e. 41.7% EC conversion with 98.1% EG and 50.2% methanol selectivities could be obtained over 25Cu@SiO₂-β-P, entry 3. These results suggest that surface areas, pore volumes of these catalysts play a weak role on the hydrogenation efficiency. One possible reason can be deduced that the unique mesoporous catalysts with flower-like nanostructures facilitated the mass transfer of the reactants, thereby leading to overcome the limit of mass transfer diffusion in the catalyst channel during reaction. As a result, the intrinsic catalytic activity was considered to play a dominant role in this case. It should be noted that the gas composition after reaction is qualitatively analyzed by Mass Spectrometer LC-D200M, and the result of mass spectrometry test is shown in the Fig S2. Besides H₂, a small amount of water, carbon monoxide, methanol, and carbon dioxide were also observed. When the copper loading was finally increased to utmost value of 45%, entry 5, 67.7% EC conversion with 97.7% EG and 52.5% methanol selectivities could be obtained over 45Cu@SiO₂-β-P. Compared to 25Cu@SiO₂-β-P, the counterpart of 25Cu@SiO₂-P without introduction of β-cyclodextrin exhibited lower catalytic activity, i.e. 30.6% EC conversion with 98.2% EG and 33.3% much lower methanol selectivity, entry 6. These results indicated that the involvement of β-cyclodextrin could effectively promoted the catalytic activity, simultaneously improved the methanol selectivity. According to the previous reports,^[16,20] it also can be deduced that Cu⁺ could stabilize the methoxy and acyl species of the reaction intermediate, and Cu⁺ could act as Lewis acidic sites to polarize the carbonyl group of EC via the interaction with the electron lone pair in oxygen, thus improving the reactivity of the cyclic ester group.

The introduction of appropriate amount of copper and additive is deemed to be crucial for obtaining higher catalyst stability. In order to evaluate the possible stability of catalyst prior to choosing the appropriate catalyst, the recycling experiments for selective hydrogenation of EC were preliminarily tested over 25Cu@SiO₂-β-P, 25Cu@SiO₂-P and 35Cu@SiO₂-β-P, and the results were shown in Table 3. Importantly, EC conversion increased to 47.4% during 2nd run over 25Cu@SiO₂-β-P, and methanol selectivity increased to 58.1% with the similar EG selectivity, entry 7. It can be speculated that induction time at the initial stage probably existed, thus active sites of 25Cu@SiO₂-β-P could be enhanced after the first run. In comparison with 25Cu@SiO₂-P catalyst, entry 8, β-cyclodextrin modified 25Cu@SiO₂-β-P exhibited higher catalytic activity during the recycling experiments, implying that the involvement of β-cyclodextrin promoted the catalyst stability. For 35Cu@SiO₂-β-P with relatively higher copper loading, the selectivities of methanol and ethylene glycol obviously decreased to 51.4% and 95.3% in the second run, respectively. According to the viewpoints by Ma et al,^[39] the catalyst powder is difficult to be shaped when the copper loading exceeded over 25% in Cu@SiO₂, which is necessary for meeting the requirement of continuous reaction mode at industrial scale. Therefore, the preliminary reusability tests showed that 25Cu@SiO₂-β-P catalyst with superior comprehensive catalytic performance was the choice for further evaluation.

Table 3. Catalytic performance of various copper-based catalysts in the hydrogenation of EC

Entry	Catalysts	EC Conv. (%)	Yield (%)		Sel. (%)	
			MeOH	EG	MeOH	EG
1	5Cu@SiO ₂ -β-P	9.4	1.2	10.8	11.0	95.2
2	15Cu@SiO ₂ -β-P	36.1	18.3	34.1	50.2	96.0
3	25Cu@SiO ₂ -β-P	41.7	21.0	39.9	50.2	98.1
4	35Cu@SiO ₂ -β-P	53.3	31.9	51.8	60.5	99.9
5	45Cu@SiO ₂ -β-P	67.7	35.5	66.1	52.5	97.7
6	25Cu@SiO ₂ -P	30.6	10.2	29.0	33.3	98.2
7	25Cu@SiO ₂ -β-P ^[a]	47.4	27.1	47.6	58.1	99.5
8	25Cu@SiO ₂ -P ^[a]	30.6	15.6	33.8	30.9	95.0
9	35Cu@SiO ₂ -β-P ^[a]	50.9	26.4	48.0	51.4	95.3

Reaction condition: 10 mmol EC, 5 MPa H₂, 20 mL THF, 20wt% catalyst dosage (based on the weight of EC), 453 K and 4 h.

[a] reused for the second run.

The effect of reaction temperature on the catalytic activity was carried out in the range of 443-483 K at 4 h, as shown in Fig. 8a. It can be seen that the EC conversion increased monotonically with the increasing reaction temperature. The EC conversion was as low as 34.1 % when the temperature was 443 K. In contrast, methanol selectivity gradually increased accompanied with elevating reaction temperature. The relatively higher EC conversion of 97.4 % was obtained when the temperature was 473 K. The EC conversion further increased to when the temperature increased to 483 K, corresponding to excellent TOF of 1195 mg_{EC}•g_{cat}⁻¹•h⁻¹. On the contrast, EG selectivity decreased to 95.5 %. This result indicated that the reaction temperature has significant influence on the catalyst behavior, and relatively higher reaction temperature was more favorable for the hydrogenation reaction. Nevertheless, too high temperature is unfavorable due to the risk of deteriorated EG selectivity. Comprehensively speaking, 473 K was chosen as the preferential reaction temperature. The influence of reaction time on the catalytic performance was also investigated, as shown in Fig 8b., 51.5 % higher EC conversion with 96.4 % EG selectivity could be obtained. The EC conversion further increased to 75.9 % at 5 h. The EC conversion increased to 92.2 % when the reaction time further prolonged to 6 h in subsequent investigation. Therefore, 25Cu@SiO₂-β-P exhibited excellent catalytic activity.

FULL PAPER

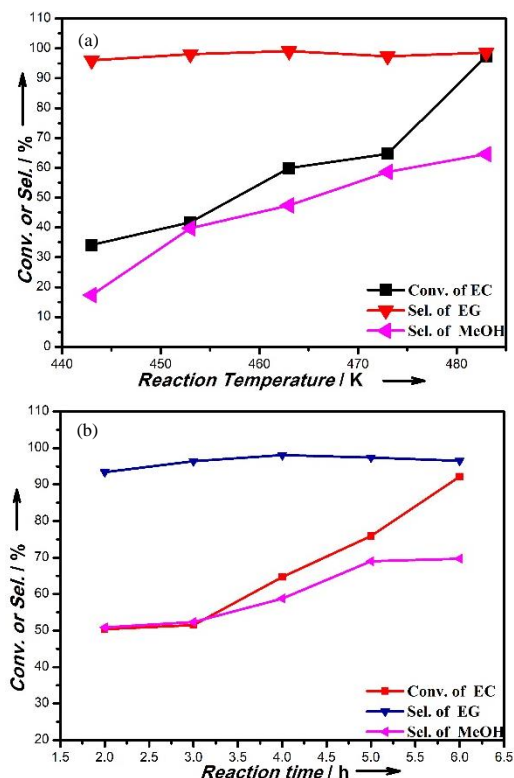


Figure 8. The effect of reaction temperature at 4 h and reaction time at 473 K on the hydrogenation of EC based on the dosage of 10mmol EC, 20 mL THF and 0.176 g $25\text{Cu}@SiO_2\text{-}\beta\text{-P}$.

The correlation of catalytic activity and structure

In order to give insights into the intrinsic active sites in the hydrogenation of ethylene carbonate, the structure-activity relationship was primarily studied. The results showed that the catalytic activity, which was expressed in terms of methanol formation rate, increased proportionally with the increment of Cu^0 active site density and attained the peak value, as shown in Fig.9. However, the methanol formation rate decreased with further increase in Cu^0 active site density, indicating the cooperative effect of Cu^0 and Cu^+ , and it could be speculated that Cu^0 played different roles in the different regions with volcano-like trend. Therefore, the correlation between the methanol formation rate and surface area of Cu^0 probably indicated that the H_2 dissociation is the rate-determining step during the reaction when Cu^0 active site density was lower than the peak value. In contrast, Cu^+ possibly played an important role in the catalytic performance for the EC hydrogenation when Cu^0 active site density exceeded, which is responsible for the polarization of C=O groups in EC.

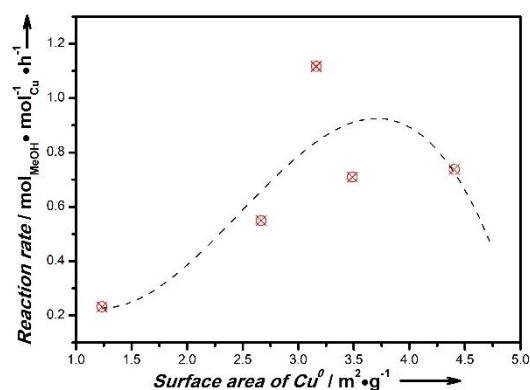
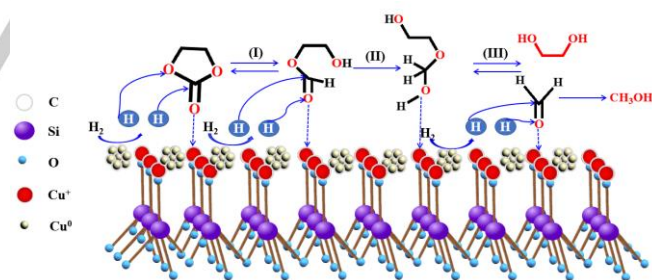


Figure 9. The correlation of between the surface Cu^0 site density and the formation rate of MeOH.

The mechanism of the hydrogenation of ethylene carbonate

Based on the analysis of the characterization of catalysts and the catalytic performance, the mechanism of EC hydrogenation to methanol and ethylene glycol over $x\text{Cu}@SiO_2\text{-}\beta\text{-P}$ catalysts was proposed, as shown in Scheme 2. Accordingly, it could be speculated that Cu^0 species was responsible for the dissociation of H_2 , while Cu^+ species polarized the C=O groups in EC. [43] Moreover, the reaction processes of EC hydrogenation could be divided to three main steps. [18] Ethylene carbonate was firstly reduced to 2-hydroxyethylformate and 1,3-dioxolan-2-ol. Subsequently, 2-hydroxyethylformate was reduced to ethylene glycol and formaldehyde. The final reduction step was the formation of methanol via the hydrogenation of formaldehyde intermediate. The existed two kinds of copper species on the catalyst surface could facilitate the hydrogenation of EC to co-produce methanol and ethylene glycol.



Scheme 2. Schematic illustration of the reaction mechanism over $x\text{Cu}@SiO_2\text{-}\beta\text{-P}$ catalysts for the hydrogenation of ethylene carbonate.

Reusability of catalysts

The stability of the copper-based catalyst is very important for the practical application in industrial scale. Unfortunately, copper-based catalyst is prone to deactivate in previous literatures. [16,44-46] The reusability of $25\text{Cu}@SiO_2\text{-}\beta\text{-P}$ was investigated at a temperature of 483K, and the result was shown in Fig. 10. In the second run of the $25\text{Cu}@SiO_2\text{-}\beta\text{-P}$, the conversion of EC slightly decreased to 95.8% which was 1.6% less than the first run, while

FULL PAPER

the selectivity of MeOH increased to 71.8% with an increment of 7.2% which can be ascribed to the excitation of the catalytic and active site. In the subsequent runs, the activity of this catalyst showed the stable performance with the selectivity of EG maintained at a high level, 97.8%, 97.7% and 97.8% hereby the conversion of EC and the selectivity of MeOH also maintained a stable level. Therefore, it can be speculated that β -cyclodextrin stabilized catalysts during the hydrogenation of EC as well as improved the catalytic activity.

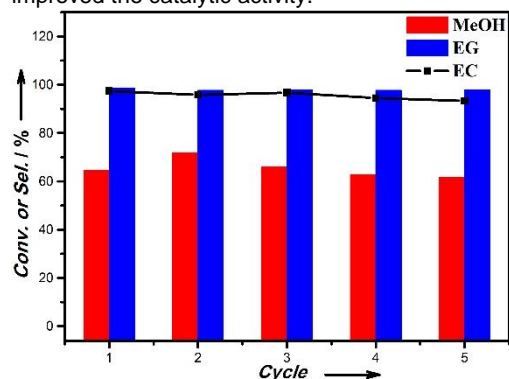


Figure 10. The reusability of 25Cu@SiO₂-β-P catalyst.

In order to explore the crucial influencing effect on catalyst stability, FT-IR, XRD, TEM and XPS characterizations of the reused catalyst 25Cu@SiO₂-β-P were performed. As identified by FT-IR (Fig. 11a), compared to the fresh catalyst, there is no noticeable change in the catalyst structure for the used catalyst. Accordingly, as revealed in Fig. 11b, the average diameter of 25Cu@SiO₂-β-P-Reused was around 1.6 nm thereby there was no change of the particle size almost, thus the β -cyclodextrin promoted catalyst exhibited marginal change in particle size during the recycling experiments. It can be deduced that the introduction of cyclodextrin could effectively inhibit the aggregation of copper particles. Connecting with the low melting point of copper with a lowing T_{Hutting} around 451 K,^[47] the catalytic activity of the traditional copper-based catalyst decreased with the reaction cycles under the high temperature. Whereas, the introduction of cyclodextrin inhibited the aggregation of catalysts which can be presumably attributed to that the residual carbon promoted the sintering temperature T_{Hutting} of catalysts and inhibited the volume diffusion of catalysts. On the contrast, the intensity of the characteristic diffraction peaks ascribable to Cu⁰ crystal plane became narrower and stronger after use (Fig. 11c), and a weaker and broader peak at around 36.2° ascribable to the Cu₂O (111) plane could be observed. Meanwhile, the distribution of Cu⁰ and Cu⁺ was further distinguished by XAES, and the Cu⁺/(Cu⁺+Cu⁰) also maintained a stable level where the reused one was 0.55, suggesting the balanced copper species was not influenced under the reaction temperature. These results indicated that the introduction of cyclodextrin promoted the stability of the catalyst effectively. The results further proved the important role of balanced Cu⁺ and Cu⁰, and the synergistic effect of these species is responsible for the superior catalytic activity.

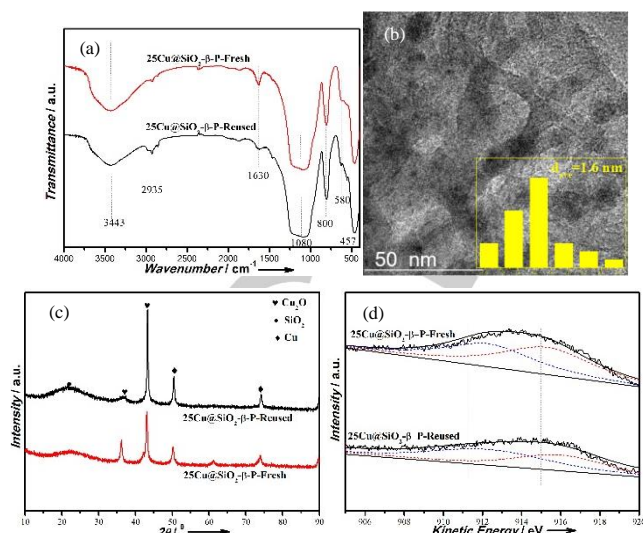


Figure 11. (a) FT-IR, (b) XRD, (c) TEM, (d) XPS of the reused 25Cu@SiO₂-β-P catalysts

Conclusions

In this study, β -cyclodextrin modified Cu@SiO₂ catalysts were prepared by a facile hydrolysis precipitation method with the assistance of P123 and was successfully applied in the hydrogenation of ethylene carbonate to co-produce methanol and ethylene glycol. In particular, mesoporous xCu@SiO₂-β-P catalyst in flower-like nanostructure were successfully prepared with sub-2 nm ultrasmall Cu particles. In addition, the Cu species are also decorated by residual carbon and confined in mesoporous silica channels. The results demonstrated that the distribution of Cu⁺ and Cu⁰ could be modulated by varying the initial copper loadings. Among the catalysts tested, the 25Cu@SiO₂-β-P catalyst exhibited relatively higher catalytic activity, and 97.4% EC conversion with 95.5% EG and 64.6% methanol selectivities could be achieved, corresponding to excellent TOF of 1195 mg_{EC}·g_{cat}⁻¹·h⁻¹. Accordingly, the relationship between the structure and activity disclosed that the maximum content of Cu⁺ species on the catalyst surface, which is beneficial for achieving superior catalytic performance. The cooperative effect between Cu⁰ and Cu⁺ species was considered to be responsible for the enhanced catalytic activity. This work has provided a new preparation method for preparing the uniformly dispersed Cu catalyst with sub-2 nm size and gives insights into the modulation method for obtaining the inexpensive copper-based catalyst with high efficiency and excellent stability, which is beneficial for the indirectly upgrading CO₂ to co-produce commodity methanol and ethylene glycol.

Experimental Section

Materials

FULL PAPER

$\text{Cu}(\text{NO}_3)_2 \cdot 3\text{H}_2\text{O}$ (>99%), β -cyclodextrin (>99%), p-xylene (>98.85%) and ammonium carbonate (>99%) were provided by Sinopharm Chemical Reagent Co., Ltd., China. Poly (ethylene glycol)-block-poly (propylene glycol)-block-poly (ethylene glycol) (P123) was purchased from Aldrich. Ethylene carbonate (EC, 99wt%) was purchased from Alfa Aesar. Tetrahydrofuran (THF, >99%) and tetraethyl silicate (TEOS) were commercially available from Xilong Chemical Co., Ltd., China. Hydrogen was provided by Beijing Haikeyuanchang Practical Gas Co., Ltd., China. Other reagents were all of analytical grade and used as received in the experiments.

Catalyst preparation

The $\text{xCu@SiO}_2\text{-}\beta\text{-P}$ catalysts (the loadings of Cu were based on the total weight of the catalyst, x=5, 15, 25, 35, 45) were synthesized by one-step hydrolysis precipitation (HP) method primarily in the presence of β -cyclodextrin and P123 and the details were described as follow.

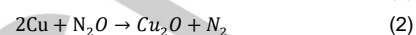
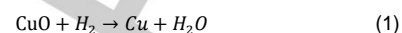
According to copper loadings, the desired weights of $\text{Cu}(\text{NO}_3)_2 \cdot 3\text{H}_2\text{O}$, 1.5 g P123 and 0.5 g β -cyclodextrin were dissolved in a mixture liquid composed of 100 mL water and 50 mL ethanol under stirring. Subsequently, the mixed solution was heated to 313 K, and 100 mL prepared ammonium carbonate aqueous liquid (0.5 mol/L) was injected into the prepared copper aqueous dropwise around 1 h. Afterwards, the corresponding weight of TEOS was dropped with the same drop velocity, hereby the temperature of liquid was maintained at 313 K simultaneously. The attained suspension was stirred for 4 h under ambient temperature when the drop process finished, thereby copper species were deposited with TEOS. After the aging stage, the suspension was heated to 363 K to evaporate ammonia until pH reached 6–7. Thereafter, the resulting suspension was filtered, washed by deionized water and ethanol in sequence for at less five times. The attained solid was dried at 363 K overnight and calcined under nitrogen atmosphere at 723 K for 4 h. Finally, the catalyst reduction was performed with 10 vol% H_2/N_2 at 623 K for 4 h, and the resulting catalysts were denoted as $\text{xCu@SiO}_2\text{-}\beta\text{-P}$. In addition, the catalyst without the introduction of β -cyclodextrin ($25\text{Cu@SiO}_2\text{-P}$) was also prepared for references.

Catalyst characterization

N_2 physisorption measurements were executed on Quantachrome Autosorb-1 at liquid nitrogen temperature (77 K) after the samples were outgassed at 573 K in vacuum for 3 h. The special surface area (S_{BET}) was determined by the Brunauer-Emmett-Teller (BET) method. The total pore volume (V_{pore}) was obtained from the absorbed volume of nitrogen with a relative pressure of 0.99. Based on the desorption branch of the isotherm, pore size distribution was preliminarily estimated by the Barrett, Joyner and Halenda (BJH) method.

The loadings of catalysts were identified by inductively coupled plasma-atomic emission spectroscopy (ICP-AES) on PerkinElmer optima 5300DV. Copper dispersity was determined by N_2O titration on a Quantachrome Chembet pulsar TPR/TPD instrument. Weight around 30 mg into quartz tube and use argon gas to purge the sample under 473 K for 1 h. After cooling to the ambient temperature, the mixture gas of 10 vol.% H_2/N_2 was introduced with the sample temperature increasing to 723 K by heating rate

of 10 K min^{-1} and maintained for 2 h. After cooling to the room temperature again, argon was introduced for purging the sample for 1 h. Then, the sample was heated to 363 K, 10 vol.% $\text{N}_2\text{O}/\text{Ar}$ was introduced under the titration model and the reaction volume of N_2O was counted until there is no change of peaks. The reactions were described by the following equations:



The copper dispersities were determined based on the actual copper loadings determined from ICP.

X-ray diffraction patterns of samples were obtained through a PANalytical Empyrean diffractometer with Cu K α radiation ($\lambda=0.15406$ nm) over 2θ range of $10^\circ - 90^\circ$.

Fourier-transform infrared spectra (FT-IR) was obtained on a Bruker Tensor 27 spectrometer. The catalyst was ground and dispersed in KBr to attain pellets utilized for FT-IR characterizations.

H_2 temperature-programmed reduction ($\text{H}_2\text{-TPR}$) studies of catalysts were performed on a Quantachrome Chembet pulsar TPR/TPD instrument. Around 30 mg calcined catalysts were pretreated with He for 1 h under 473 K, and the aforementioned sample was cooled to room temperature before reduction process. Subsequently, the TPR was implemented from 323 K to 803 K with a heating rate of 10 $\text{K}\cdot\text{min}^{-1}$ by introducing 10 vol% H_2/N_2 .

Transmission electron microscopy (TEM) and high-resolution transmission electron microscopy (HRTEM) images were attained by field-emission transmission electron microscopy (JEOL, JEM-2100F), which was operated at an acceleration voltage of 200 kV to characterize the morphologies and the crystal structures of the xCu@SiO_2 . Prior to the investigation, the samples were ultrasonically dispersed in ethanol at room temperature for around 30 min. The scanning mode was employed together with EDX spectroscopy. Afterwards, the suspension was deposited on copper grids supported by holey carbon films, and the measurement was tested after the sample drying.

X-ray photoelectron spectroscopy (XPS) and X-ray Auger electron spectroscopy (XAES) were employed to probe the surface chemical states of samples. The equipment was conducted under an ultrahigh vacuum using an ESCALAB 259Xi spectrometer with Al K α radiation (1486.6 eV) and a multichannel detector. The obtained binding energies were calibrated by using C1s peak at 284.6 eV as the reference with an uncertainty of ± 0.2 eV.

Catalyst performance tests

The catalytic activities of the xCu@SiO_2 catalysts were implemented for the hydrogenation of EC in a 50 mL stainless steel autoclave under magnetic stirring. Typically, 10 mmol EC, 20 mL THF and 0.176 g catalyst were weighted and introduced into the autoclave. After the autoclave sealed and flushed repeatedly with H_2 five times, the autoclave was charged with 5 MPa H_2 . The reactor was heated to the desired temperature for a desired time with a magnetic stirring rate of 550 rpm. After the reaction finished, the autoclave was cooled to the ambient temperature by ice-water. The residual hydrogen was released to atmosphere carefully. The quantitative analysis of the reaction mixture was measured on Shimadzu GC-2014 with a GsBP-1 column (30 $\text{m} \times 0.32$ $\text{mm} \times 1.0$ μm) and a flame

FULL PAPER

ionization detector (FID) using p-xylene as the internal standard. As for the recycling experiments, the catalyst was separated by centrifugation, washed by THF for five times. The obtained catalysts were designated as 25Cu@SiO₂-β-P-Reused and used for the next run.

Acknowledgements

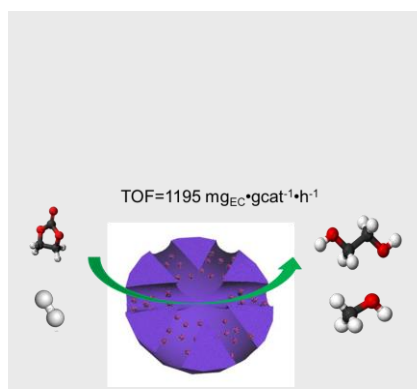
We are grateful to the National Natural Science Foundation of China (21576272), "Transformational Technologies for Clean Energy and Demonstration", Strategic Priority Research Program of the Chinese Academy of Sciences, Grant No. XDA 21030600, and the project from Jiangsu Collaborative Innovation Center for Ecological Building Materials and Environmental Protection Equipment (YCXT201607) for the financial supports.

Keywords: Carbon dioxide • Ethylene Carbonate • Mesoporous Cu@SiO₂ • Methanol • Ethylene glycol

- [1] N. Von der Assen, A. Sternberg, A. Katelhon, A. Bardow, *Faraday Discuss* **2015**, *183*, 291-307.
- [2] Q. Shen, J. Ma, X.F. Huang, N.J. Yang, G.H. Zhao *Appl. Catal. B: Environ.* **2017**, *219*, 45–52.
- [3] Y. J. Jang, J. Jang, J. Lee, J.H. Kim, H. Kumagai, J. Lee, T. Minegishi, J. Kubota, K. Domen, J. S. Lee *Energy Environ. Sci.* **2015**, *8*, 3597–3604.
- [4] L. Gu, Y. Qin, Y. Gao, X. Wang, F. Wang *Chin. J. Chem.* **2012**, *30*, 2121-2125.
- [5] H. F. Jiang, B. Z. Yuan *Chin. J. Chem.* **2010**, *26*, 1305-1308.
- [6] X. Dong, F. Li, N. Zhao, Y. Tan, J. Wang, F. Xiao *Chin. J. Catal.* **2017**, *38*, 717-725.
- [7] C. Gundanathan, D. Milstein *Chem. Rev.* **2014**, *114*, 12024-12087
- [8] S. Werkmeister, J. Neumann, K. Junge, M. Beller *Chem. Eur. J.* **2015**, *21*, 12226-12250.
- [9] Q. W. Song, Z. H. Zhou, L. N. He *Green Chem.* **2017**, *19*, 3707-3728
- [10] G. A. Olah *Angew. Chem., Int. Ed.* **2005**, *44*, 2636-2639
- [11] G. A. Olah, A. Goepfert, G. K. S. Prakash *Beyond Oil and Gas: The Meth. Eco.*, 2nd edn, **2009**.
- [12] D. R. Palo, R. A. Dagle, J. D. Holladay *Chem. Rev.* **2007**, *107*, 3992-4021
- [13] M. Y. He, Y. H. Sun, B. X. Han *Angew. Chem., Int. Ed.* **2013**, *52*, 9620.
- [14] G. Song, H. Yang, Y. Sun, J. Wang, W. Qu, Q. Zhang, L. Ma, Y. Feng *Chin. J. Catal.* **2017**, *38*, 554-562.
- [15] C. Qiao, X. F. Liu, X. Liu, L. N. He *Org. Lett.* **2017**, *19*, 1490-1493.
- [16] F. J. Li, L. G. Wang, X. Han, Y. Cao, P. He, H. Q. Li *Int. J. Hydrogen Energy* **2017**, *42*, 2144-2156.
- [17] Y. Cui, X. Chen, W. Dai *RSC Adv.* **2016**, *6*, 69530-69539.
- [18] Z. B. Han, L. C. Rong, J. Wu, L. Zhang, Z. Wang, K. L. Ding *Angew. Chem., Int. Ed.* **2012**, *51*, 13041.
- [19] Y. H. Li, K. Junge, M. Beller *Chem. Cat. Chem.* **2013**, *5*, 1072
- [20] F.J. Li, L. G. Wang, X. Han, P. He, Y. Cao, H. Q. Li *RSC Adv.* **2016**, *6*, 45894-45906.
- [21] Y. Wang, Y. Shen, Y. Zhao, J. Lv, S. Wang, X. Ma *ACS Catal.* **2015**, *5*, 6200–6208
- [22] S. Zhu, X. Gao, Y. Zhu, W. Fan, J. Wang, Y. Li *Catal. Sci. Technol.* **2015**, *5*, 1169–1180
- [23] Z. Q. Wang, Z. N. Xu, S. Y. Peng, M. J. Zhang, G. Lu, Q. S. Chen, Y. Chen, G. C. Guo *ACS Catal.* **2015**, *5*, 4255–4259
- [24] L. F. Chen, P. J. Guo, M. H. Qiao, S. R. Yan, H. X. Li, W. Shen, H. L. Xu, K. N. Fan *J. Catal.* **2008**, *257*, 172–180.
- [25] S. Li, Y. Wang, J. Zhang, S. Wang, Y. Xu, Y. Zhao, X. Ma *Ind. Eng. Chem. Res.* **2015**, *54*, 1243-1250.
- [26] J. Gong, H. Yue, Y. Zhao, S. Zhao, L. Zhao, J. Lv, S. Wang, X. Ma *J. Am. Chem. Soc.* **2012**, *134* 13922-13925.
- [27] C. Lian, F. Ren, Y. Liu, G. Zhao, Y. Ji, H. Rong, W. Jia, L. Ma, H. Lu, D. Wang, Y. Li *Chem. Commun.* **2015**, *51*, 1252-1254
- [28] H. Liu, Z. Huang, Z. Han, K. Ding, H. Liu, C. Xia, J. Chen *Green Chem.* **2015**, *17*, 4281-4290.
- [29] X. Chen, Y. Cui, C. Wen, B. Wang, W. L. Dai *Chem. Commun.* **2015**, *51*, 13776-13778.
- [30] R. P. Ye, L. Lin, J. X. Yang, M. L. Sun, F. Li, B. Li *J. Catal.* **2017**, *350*, 122-132.
- [31] Y. J. Zhao, Z. Y. Guo, H. J. Zhang, Y. X. Xu, Y. Wang, J. Zhang, Y. Xu, S. P. Wang, X. B. Ma *Chem. Lett.* **2017**, *46*, 1079-1082.
- [32] Y. J. Zhao, Z. Y. Guo, H. J. Zhang, B. Peng, Y. X. Xu, Y. Wang, J. Zhang, Y. Xu, X. B. Ma, *J. Catal.* **2018**, *357*, 223-237.
- [33] A. Z. Badruddoza, A. S. Tay, P. Y. Tan, K. Hidajat, M. S. Uddin *J. Hazard. Mater.* **2011**, *185*, 1177-1186.
- [34] Z. Huang, F. Cui, H. Kang, J. Chen, X. Zhang, C. Xia, *Chem. Mater.* **2008**, *20*, 5090-5099
- [35] Y. Li, L. Tang, X. Ma, X. Wang, W. Zhou, D. Bai *J. Phys. Chem. Solids* **2017**, *107*, 62-67.
- [36] M. Wang, G. Fang, P. Liu, D. Zhou, C. Ma, D. Zhang, J. Zhan *Appl. Catal. B: Environ.* **2016**, *188*, 113-122.
- [37] M. Tamura, T. Kitanaka, Y. Nakagawa, K. Tomishige *ACS Catal.* **2015**, *6*, 376-380.
- [38] L. He, H. Cheng, G. Liang, Y. Yu, F. Zhao *Appl. Catal.* **2013**, *452*, 88–93.
- [39] Y. Zhao, S. Li, Y. Wang, B. Shan, J. Zhang, S. Wang, X. Ma *Chem. Eng. J.* **2017**, *313*, 759-768.
- [40] T. Ding, H. Tian, J. Liu, W. Wu, J. Yu *Chin. J. Catal.* **2016**, *37*, 484-493.
- [41] C. Wen, F. Li, Y. Cui, W. L. Dai, K. Fan *Catal. Today.* **2014**, *233*, 117-126.
- [42] H. Lin, X. Zheng, Z. He, J. Zheng, X. Duan, Y. Yuan *Appl. Catal. A* **2012**, *445*, 287-296.
- [43] M. M. Zhou, Y. F. Shi, K. Ma, S. Y. Tang, C. J. Liu, H. R. Yue, B. Liang *Ind. Eng. Chem. Res.* **2018**, *57*, 1924-1934
- [44] D. Wang, Y. Tan, Y. Han, T. Noritatsu *Chin. J. Catal.* **2008**, *29*, 63-68.
- [45] S. Natesakhawat, P. R. Ohodnicki, B. H. Howard, J. W. Lekse, J. P. Baltrus, C. Matranga *Topics in Catalysis* **2013**, *56*, 1752-1763.
- [46] X. Y. Zhang, M. H. Wang, Z. Y. Chen, P. Xiao, P. Webley, Y. C. Zhai *Journal of Central South University* **2018**, *25*, 691-700.
- [47] Z. Huang, F. Cui, J. Xue, J. Zuo, J. Chen, C. J. Xia *Phys. Chem. C* **2010**, *114*, 16104-16113

FULL PAPER

β -cyclodextrin modified Cu@SiO₂ catalysts were prepared by a facile hydrolysis precipitation method and was successfully applied in the co-production of methanol and ethylene glycol via hydrogenation of ethylene carbonate derived from CO₂.



Chanjuan Zhang^{a,b,c,d}, Ligu Wang^{a,c,d*},
Jiaju Liu^a, Yanmi Yang^a, Peng He^a, Yan
Cao^a, Jiaqiang Chen^a, Huiquan Li^{a,c,d*}

Page No. – Page No.

Facile fabrication of ultrasmall copper species confined in mesoporous silica for chemo-selective and stable hydrogenation ethylene carbonate derived from CO₂